Mobility Aware CSI Reliability in PASS Assisted Highway V2I Systems

Ura Modi, Student Member, IEEE, and Dhaval K. Patel, Senior Member, IEEE
School of Engineering and Applied Science, Ahmedabad University, Ahmedabad, India
{ura.m, dhaval.patel}@ahduni.edu.in

***Abstract*—High-mobility V2I channels are significantly impacted by CSI aging, which can result in a non-zero outage floor even at high SNR. In this paper, we investigate waveguide-based pinching antenna systems (PASS) for highway V2I communication, where a movable radiator along the roadside waveguide partially follows vehicular motion to control the residual Doppler spread. We focus on a highway regime with LoS-favorable geometry and model the residual small-scale fluctuation as Rayleigh-equivalent fading for tractability. Under an equivalent-SNR approximation, we obtain a conditional outage law and characterize the high-SNR outage floor. We then propose a fairness-oriented reliability requirement based on the α-quantile of the long-term user outage and develop a low-complexity two-timescale policy for motion control, pilot updating, and scheduling. Simulation results validate the analysis and demonstrate the benefits of the proposed joint PASS framework.**

***Index Terms*—CSI aging, highway V2I, outage probability, pinching-antenna systems, residual Doppler.**

I. Introduction

High-frequency vehicle-to-infrastructure (V2I) communications are significantly affected by rapid channel variation, beam sensitivity, and channel state information (CSI) aging under vehicular mobility. Mobility-aware beam management and CSI acquisition/aging in reconfigurable wireless systems were investigated in recent studies [1]–[3]. However, such techniques are based on fixed radiating points.

Pinching antenna systems (PASS) have recently emerged as a flexible architecture in which dielectric waveguides act as low-loss guided transmission media, and pinching antennas radiate electromagnetic waves from arbitrary points along the waveguide [4]–[6]. Existing PASS studies provide analytical tools for performance analysis, attenuation-aware placement, and channel estimation [7]–[9]. However, these studies mainly optimize the placement of the PA for quasi-static user geometries and average-performance metrics, rather than reliability in highway V2I systems.

The reason behind writing this paper is due to the fact that CSI fading is caused mainly because of Doppler effect. The movability of the PASS radiator along the roadside waveguide enables it to somewhat track the trajectory of the vehicle, thereby compensating for the Doppler of the link, as well as maintaining communication geometry. The small-scale fluctuations around this geometry are modeled by a Rayleigh-equivalent residual fading term, as in [10]. The main contributions are as follows:

- To the best of our knowledge, this paper is the first attempt that treats the mobility of a pinching-antenna radiator as a knob to control CSI reliability in high-mobility V2I, whereby radiator mobility is exploited to mitigate the residual Doppler.
- We develop a model for the residual Doppler in the waveguide-fed movable radiator and, based on it, formulate a new CSI reliability measure that combines pilot quality and Doppler-induced aging into a single scalar.
- Leveraging this scalar measure, we derive the equivalent-SNR (signal-to-noise ratio) outage rule, prove the existence of an outage floor due to the actuator limit in the high-SNR regime, and provide a sufficient condition under which this actuator-limited floor is positive.
- A reduced-complexity two-timescale framework is proposed to control the movement of the radiator, the updating of pilots, and the scheduling process under fairness-aware quantile-reliability criteria, and is verified via Monte-Carlo simulations that demonstrate the correctness of the analytical outage-probability formula.

II. System Model

We consider a straight highway segment of length D meters. A dielectric waveguide is deployed along the roadside, parallel to the road, and aligned with the y-axis over $y \in [0, D]$, as illustrated in Fig. 1. A feed unit at $y = 0$ launches the radio-frequency (RF) signal into the waveguide. Let K vehicles travel along the road, indexed by $k = 1, \ldots, K$. A pinching antenna (PA) extracts power from the waveguide and radiates it toward the wireless channel. At time t, its longitudinal and 3D positions are $y_r(t) \in [0, D]$ and $\mathbf{p}_r(t) = [x_r,\, y_r(t),\, h_r]^T$, respectively, where x_r is the lateral distance from the center of the road and h_r is the PA height. We consider a single-cell time-division multiple access (TDMA) downlink, where at most one vehicle is served in each transmission slot. Channel acquisition occurs based on periodic pilot transmission on the uplink every ΔT_p seconds via time-division duplex (TDD) reciprocity. Here, $y_r(t)$ represents the longitudinal position of the movable PA, whose motion satisfies $\dot{y}_r(t) = u(t)$ with $|u(t)| \le v_r^{\max}$. Let $y_k(t)$ denote the longitudinal position of vehicle k, with $\mathbf{p}_k(t) = [0,\, y_k(t),\, 0]^T$ and $v_k(t) = \dot{y}_k(t)$. The PA–vehicle distance is $d_k(t) = \|\mathbf{p}_k(t) - \mathbf{p}_r(t)\|$. If $P_{\mathrm{in}}(t)$ denotes the RF power launched into the waveguide, then the guided power available at PA position $y_r(t)$ is $P_{\mathrm{wg}}(t) = P_{\mathrm{in}}(t) 10^{-\alpha_{\mathrm{wg}} y_r(t)/10}$, where α_{wg} (dB/m) is the waveguide attenuation coefficient. The radiated power is modeled as $P_{\mathrm{rad}}(t) = \eta_c P_{\mathrm{wg}}(t)$, where $\eta_c \in (0, 1]$ is the effective PA

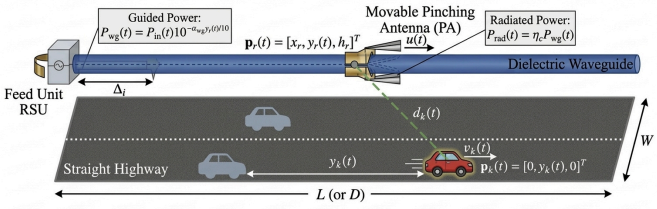

Fig. 1. System model of the dielectric waveguide communication setup with a pinching antenna (PA) serving a scheduled vehicle traveling along the highway.

efficiency. The large-scale pathloss is modeled as $PL_k(t) = FSPL(1\,\mathrm{m}) + 10\nu \log_{10}\big(d_k(t)\big) + X_\sigma$, where ν is the pathloss exponent, $FSPL$ denotes the free-space path loss, and $X_\sigma \sim \mathcal{N}(0, \sigma_{\mathrm{sh}}^2)$ models lognormal shadowing. Thus, the linear-scale large-scale power gain is given by $\beta_k(t) = 10^{-PL_k(t)/10}$. The complex baseband downlink channel from the PA to vehicle k is $h_k(t) = \sqrt{\beta_k(t)}\, g_k(t)$, where $g_k(t)$ represents the small-scale fading.

Our focus is on a highway regime in which PASS mobility maintains a favorable propagation geometry by optimally placing the radiator. For tractability, the small-scale fluctuation about this geometry is captured by a single Rayleigh-equivalent fading term, $g_k(t) \sim \mathcal{CN}(0,1)$, or equivalently $|g_k(t)|^2 \sim \mathrm{Exp}(1)$. The fading is assumed to remain constant within each transmission slot of duration Δt. We do not explicitly model strong Rician or line-of-sight (LoS) components, blockage, or non-stationary scattering. Since the radiator is placed to keep a favorable LoS geometry, the Rayleigh-equivalent term is only meant to describe the residual fading around that geometry, and the Rician and LoS/non-line-of-sight (NLoS)-blockage case is left for future work.

III. Residual Doppler and CSI Reliability

Let $\mathbf{r}_k(t) = \mathbf{p}_k(t) - \mathbf{p}_r(t)$ denote the displacement between vehicle k and the movable radiator, and let $\hat{\mathbf{r}}_k(t) = \mathbf{r}_k(t)/\|\mathbf{r}_k(t)\|$. The relative radial velocity is

$$v_{\mathrm{rel},k}(t) = \hat{\mathbf{r}}_k^T(t)\big(\dot{\mathbf{p}}_k(t) - \dot{\mathbf{p}}_r(t)\big). \tag{1}$$

Hence, the Doppler shift is $f_{D,k}(t) = v_{\mathrm{rel},k}(t)/\lambda$, where $\lambda = c/f_c$. Since both the vehicle and the radiator primarily move along the highway axis, (1) becomes

$$f_{D,k}(t) = \frac{\big(v_k(t) - \dot{y}_r(t)\big)\cos\phi_k(t)}{\lambda}, \tag{2}$$

where

$$\cos\phi_k(t) = \frac{y_k(t) - y_r(t)}{\sqrt{x_r^2 + h_r^2 + \big(y_k(t) - y_r(t)\big)^2}}. \tag{3}$$

Thus, PASS can reduce the residual Doppler by reducing the speed mismatch $|v_k(t) - \dot{y}_r(t)|$ through radiator motion. A constant Doppler component is just an offset in the carrier frequency and can be compensated by normal synchronization techniques. So in the above equation, $f_{D,k}(t)$ refers to the Doppler spread due to scatterers and small geometrical offsets in the neighborhood of the LoS position, which is responsible for reducing the correlation time in (4), hence the high-SNR outage floor.

CSI is refreshed every ΔT_p seconds. Let

$$\eta_{\mathrm{CSI}} = \frac{\rho_p \tau_p}{1 + \rho_p \tau_p},$$

where ρ_p and τ_p denote the pilot SNR and pilot length, respectively. Under the adopted Rayleigh-equivalent fading model, if $\Delta t_{\mathrm{CSI}}(t) \in [0, \Delta T_p]$ denotes the CSI age, then we use the classical Clarke-type temporal-correlation model [11], which is also standard in CSI-aging analyses [3]:

$$\rho_k(\Delta t_{\mathrm{CSI}}(t)) = J_0(2\pi f_{D,k}(t)\Delta t_{\mathrm{CSI}}(t)), \tag{4}$$

where $J_0(\cdot)$ is the zeroth-order Bessel function. We define the CSI reliability factor as

$$\psi_k(t) = \eta_{\mathrm{CSI}}\,|\rho_k(\Delta t_{\mathrm{CSI}}(t))|^2, \qquad 0 \le \psi_k(t) \le 1. \tag{5}$$

Thus, the quality of the pilot signals and the CSI aging effects are reflected in $\psi_k(t)$, which depends on f_c, $v_k(t)$, $\dot{y}_r(t)$, $\phi_k(t)$, and ΔT_p. In practice, η_{CSI} follows from the pilot SNR ρ_p and pilot length τ_p, while $|\rho_k(\Delta t_{\mathrm{CSI}})|$ can be found from $f_{D,k}$ using the tracked vehicle speed and geometry, or simply by measuring the correlation between successive channel estimates.

The constraint on the Doppler compensation is due to the limited speed of the actuator. From the inequality

$$|v_k(t) - \dot{y}_r(t)| \ge \max\{|v_k(t)| - v_r^{\max}, 0\},$$

we obtain

$$|f_{D,k}(t)| \ge \frac{\max\{|v_k(t)| - v_r^{\max}, 0\}\,|\cos\phi_k(t)|}{\lambda}. \tag{6}$$

On a straight road both the vehicle and the radiator move mainly along the road axis, so only the longitudinal velocity enters (2). Using the evenness of $J_0(\cdot)$, we define

$$\zeta_k(t) \triangleq \frac{2\pi\Delta t_{\mathrm{CSI}}(t)}{\lambda}\max\{|v_k(t)| - v_r^{\max}, 0\}\,|\cos\phi_k(t)|. \tag{7}$$

Here $\zeta_k(t)$ is the actuator-limited lower bound on the Doppler-correlation argument, i.e., $2\pi|f_{D,k}(t)|\,\Delta t_{\mathrm{CSI}}(t) \ge \zeta_k(t)$. Since $J_0^2(x)$ is not monotone on $[0,\infty)$, we define

$$\mathcal{U}(z) \triangleq \sup_{x \ge z} J_0^2(x), \qquad z \ge 0.$$

Hence,

$$\psi_k(t) \le \eta_{\mathrm{CSI}}\,\mathcal{U}\big(\zeta_k(t)\big). \tag{8}$$

Since $J_0^2(\cdot)$ is not monotone, taking the supremum over $x \ge \zeta_k(t)$ keeps the largest reliability still allowed by the actuator-limited argument, so (8) is the tightest bound we can guarantee once the actuator can no longer match the vehicle speed ($|v_k(t)| > v_r^{\max}$).

IV. Outage Analysis and High-SNR Asymptotics

For slotted downlink transmission, let $n \in \{1, \ldots, N\}$ denote the slot index and $k_n \in \{1, \ldots, K\}$ the user scheduled in the nth slot. The nominal instantaneous SNR of user k in slot n is defined as

$$\gamma_k[n] = \frac{P_{\mathrm{rad}}[n]\beta_k[n]|g_k[n]|^2}{\sigma^2}, \tag{9}$$

where σ^2 denotes the receiver noise power.

The relation between CSI reliability and detector performance is given by

$$h_k[n] = \sqrt{\psi_k[n]}\,\hat{h}_k[n] + \sqrt{1 - \psi_k[n]}\,\tilde{h}_k[n], \tag{10}$$

where $\hat{h}_k[n]$ is the known (estimated) channel component and $\tilde{h}_k[n]$ is the residual uncertainty, where $\hat{h}_k[n]$ and $\tilde{h}_k[n]$

are uncorrelated and $\mathbb{E}[|\hat{h}_k[n]|^2] = \mathbb{E}[|\tilde{h}_k[n]|^2] = \beta_k[n]$. Using an equivalent-SNR approximation in which the residual uncertainty is treated as Gaussian self-interference, we obtain the effective-SNR model

$$\gamma_k^{\mathrm{eff}}[n] = \frac{\psi_k[n]\gamma_k[n]}{1 + \big(1 - \psi_k[n]\big)\gamma_k[n]}. \tag{11}$$

Modeling $\tilde{h}_k[n]$ as Gaussian self-interference is the usual worst-case choice in CSI-error analysis, since for a given error variance Gaussian interference is the least favorable for the rate. Equation (11) therefore gives a conservative, lower-bound effective SNR rather than the exact value for a specific detector.

Lemma 1. *For $\gamma \geq 0$, $\gamma^{\mathrm{eff}}(\psi, \gamma)$ is strictly increasing in $\psi \in [0, 1]$. For $\psi \in (0, 1]$, it is strictly increasing in $\gamma \geq 0$.*

Proof. For $\gamma^{\mathrm{eff}}(\psi, \gamma) = \psi\gamma/(1+(1-\psi)\gamma)$, we have $\partial_\psi \gamma^{\mathrm{eff}} = \frac{\gamma(1+\gamma)}{(1+(1-\psi)\gamma)^2} > 0$ and $\partial_\gamma \gamma^{\mathrm{eff}} = \frac{\psi}{(1+(1-\psi)\gamma)^2} > 0$. Hence, γ^{eff} is increasing in ψ for $\gamma \geq 0$ and in γ for $\psi \in (0, 1]$.

Let R_k be the target spectral efficiency of user k and $\tau_k = 2^{R_k} - 1$ represent the outage threshold. Then $\gamma_k^{\mathrm{eff}}[n] < \tau_k$ is equivalent to $((1 + \tau_k)\psi_k[n] - \tau_k)\gamma_k[n] < \tau_k$. Hence, if $\psi_k[n] \leq \tau_k/(1 + \tau_k)$, outage occurs with probability one; otherwise,

$$\Gamma_k[n] \triangleq \frac{\tau_k}{(1 + \tau_k)\psi_k[n] - \tau_k}, \qquad \gamma_k[n] < \Gamma_k[n]. \tag{12}$$

Under the Rayleigh-equivalent model, $|g_k[n]|^2 \sim \mathrm{Exp}(1)$, so $\gamma_k[n]$ is exponential with mean $\bar{\gamma}_k[n] = P_{\mathrm{rad}}[n]\beta_k[n]/\sigma^2$. Therefore,

$$P_{\mathrm{out},k}[n \mid \psi_k[n]] = \begin{cases} 1 - \exp\left(-\dfrac{\Gamma_k[n]}{\bar{\gamma}_k[n]}\right), & \psi_k[n] > \dfrac{\tau_k}{1 + \tau_k}, \\ 1, & \psi_k[n] \leq \dfrac{\tau_k}{1 + \tau_k}. \end{cases} \tag{13}$$

Thus, CSI reliability controls both the required nominal-SNR threshold $\Gamma_k[n]$ and the sure-outage region $\psi_k[n] \leq \tau_k/(1 + \tau_k)$.

Proposition 1 (Effective-SNR ceiling)**.** *For fixed $\psi \in [0, 1)$, the effective SNR saturates as*

$$\lim_{\gamma \to \infty} \gamma^{\mathrm{eff}}(\psi, \gamma) = \frac{\psi}{1 - \psi}. \tag{14}$$

Proof.

$$\gamma^{\mathrm{eff}}(\psi, \gamma) = \frac{\psi}{\gamma^{-1} + (1 - \psi)} \xrightarrow[\gamma \to \infty]{} \frac{\psi}{1 - \psi}.$$

Proposition 2 (Outage floor)**.** *As $\bar{\gamma}_k[n] \to \infty$, the outage probability converges to*

$$P_{\mathrm{out},k}[n] \to \Pr\left(\psi_k[n] \leq \frac{\tau_k}{1 + \tau_k}\right). \tag{15}$$

Proof. From (13),

$$P_{\mathrm{out},k}[n] = \mathbb{E}\Big[\mathbf{1}_{\{\psi_k[n] \leq \frac{\tau_k}{1+\tau_k}\}}\Big] + \mathbb{E}\Big[\Big(1 - e^{-\Gamma_k[n]/\bar{\gamma}_k[n]}\Big)\mathbf{1}_{\{\psi_k[n] > \frac{\tau_k}{1+\tau_k}\}}\Big].$$

where $\mathbf{1}_{\{\mathcal{A}\}}$ denotes the indicator of event $\mathcal{A}$. The second term vanishes as $\bar{\gamma}_k[n] \to \infty$, which yields (15).

The floor in Proposition 2 depends only on $\psi_k[n]$, not on the distribution of $g_k[n]$: whenever $|g_k[n]|^2$ has no point mass at zero (as for Rician or Nakagami fading), the pre-floor term vanishes as $\bar{\gamma}_k[n] \to \infty$, leaving the same floor $\Pr(\psi_k[n] \leq \tau_k/(1 + \tau_k))$. Only the pre-floor curve changes with the fading model, so the high-SNR floor is robust to the LoS/Rician structure of the channel.

Using Proposition 2 and (8), we have the following corollary.

Corollary 1. *Let*

$$\zeta_k[n] \triangleq \frac{2\pi\Delta t_{\mathrm{CSI}}[n]}{\lambda} \max\{|v_k[n]| - v_r^{\max}, 0\}\,|\cos\phi_k[n]|. \tag{16}$$

If

$$\Pr\left(\eta_{\mathrm{CSI}}\,\mathcal{U}\big(\zeta_k[n]\big) < \frac{\tau_k}{1 + \tau_k}\right) > 0, \tag{17}$$

then the high-SNR outage floor of user k is strictly positive.

Proof. On the event in (17), (8) implies

$$\psi_k[n] < \frac{\tau_k}{1 + \tau_k},$$

and the claim follows from Proposition 2.

V. Mobility-Aware PASS Control

Let $\pi = (\{y_r[n]\}, \{k_n\}, \Delta T_p)$ denote the radiator trajectory, scheduling sequence, and pilot-update period. Over a horizon of N slots, define the service count

$$S_k^{(N)}(\pi) = \sum_{n=1}^{N} \mathbf{1}_{\{k_n = k\}},$$

and the empirical outage

$$\hat{P}_{\mathrm{out},k}^{(N)}(\pi) = \begin{cases} \dfrac{\sum_{n=1}^{N} \mathbf{1}_{\{k_n = k,\ \gamma_k^{\mathrm{eff}}[n] < \tau_k\}}}{S_k^{(N)}(\pi)}, & S_k^{(N)}(\pi) > 0, \\ 1, & S_k^{(N)}(\pi) = 0. \end{cases}$$

The long-term outage probability is

$$\bar{P}_{\mathrm{out},k}(\pi) = \limsup_{N \to \infty} \hat{P}_{\mathrm{out},k}^{(N)}(\pi). \tag{18}$$

To capture fairness-sensitive reliability, we adopt the α-quantile functional

$$J_\alpha(\pi) = \inf\left\{z \in \mathbb{R}_+ : \frac{1}{K}\sum_{k=1}^{K} \mathbf{1}_{\{\bar{P}_{\mathrm{out},k}(\pi) \leq z\}} \geq \alpha\right\}. \tag{19}$$

The reliability optimization problem is

$$\begin{aligned} \min_{\{y_r[n]\}, \{k_n\}, \Delta T_p} \quad & J_\alpha(\pi) \\ \text{s.t.} \quad & 0 \leq y_r[n] \leq D,\ \forall n, \\ & |y_r[n+1] - y_r[n]| \leq v_r^{\max}\Delta t,\ \forall n, \\ & \Delta T_p \in \mathcal{T}, \\ & k_n \in \{1, \ldots, K\},\ \forall n. \end{aligned} \tag{20}$$

Problem (20) is non-convex due to the nonlinear dependence of $\gamma_k^{\mathrm{eff}}[n]$ on $\psi_k[n]$, as well as the dependence of $\psi_k[n]$ on residual Doppler geometry, actuator motion, and CSI age. Moreover, the non-smooth objective in $J_\alpha(\pi)$ spans a long time horizon among users. We propose a low-complexity two-timescale surrogate motivated by the outage structure in (13) and the high-SNR behavior in (14)–(15).

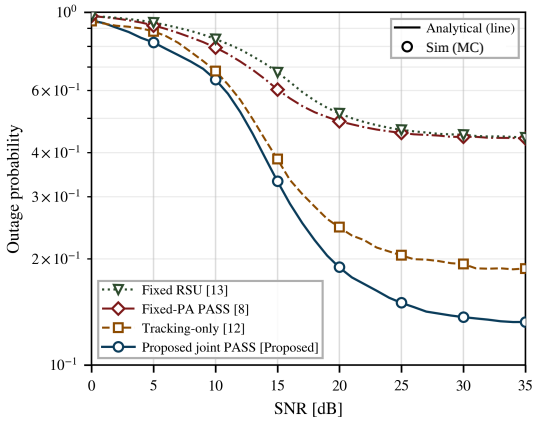

Fig. 2. Outage probability versus nominal SNR for $\Delta T_p = 1$ ms. Lines denote the closed-form law in (13) and markers denote Monte Carlo simulation.

Let $\hat{J}_\alpha^{(N)}(\pi)$ denote the empirical counterpart of (19), obtained by replacing $\bar{P}_{\mathrm{out},k}(\pi)$ with $\hat{P}_{\mathrm{out},k}^{(N)}(\pi)$. On the slow timescale, the pilot period is selected as

$$\Delta T_p^\star = \arg\min_{\Delta T_p \in \mathcal{T}} \hat{J}_\alpha^{(N)}\big(\pi(\Delta T_p)\big). \tag{21}$$

Since $\mathcal{T}$ is finite, (21) is a direct search over the candidate periods.

On the fast timescale, scheduling uses the PASS-aware proportional-fair score, where $\bar{q}_k[n]$ is the running-average goodput of user k from (23) and serves as the proportional-fair weight,

$$\mathrm{score}_k[n] = \frac{\psi_k[n]\bar{\gamma}_k[n]}{\bar{q}_k[n]+\varepsilon}, \qquad \bar{\gamma}_k[n] = \frac{P_{\mathrm{rad}}[n]\beta_k[n]}{\sigma^2}, \tag{22}$$

where $\varepsilon > 0$ avoids division by zero.

Proposition 3 (Scheduler score as an outage surrogate)**.** *For fixed $\bar{q}_k[n]+\varepsilon > 0$, the score in* (22) *is strictly increasing in both $\psi_k[n]$ and $\bar{\gamma}_k[n]$. Moreover, for $\psi_k[n] > \tau_k/(1+\tau_k)$, the conditional outage probability in* (13) *is strictly decreasing in both $\psi_k[n]$ and $\bar{\gamma}_k[n]$. Hence, under the adopted model, maximizing* (22) *favors users with smaller one-step conditional outage outside the sure-outage region, while $\bar{q}_k[n]+\varepsilon$ provides proportional-fair regularization.*

Proof. The first claim follows directly from (22). For the second, when $\psi_k[n] > \tau_k/(1+\tau_k)$, we have $P_{\mathrm{out},k}[n \mid \psi_k[n]] = 1 - \exp\!\Big(-\frac{\Gamma_k[n]}{\bar{\gamma}_k[n]}\Big)$, where $\Gamma_k[n] = \frac{\tau_k}{(1+\tau_k)\psi_k[n]-\tau_k}$. Direct differentiation shows that $\Gamma_k[n]$ decreases in $\psi_k[n]$, while $P_{\mathrm{out},k}[n \mid \psi_k[n]]$ decreases in both $\Gamma_k[n]$ and $\bar{\gamma}_k[n]$. Hence it decreases in both $\psi_k[n]$ and $\bar{\gamma}_k[n]$. When $\psi_k[n] \le \tau_k/(1+\tau_k)$, (13) yields unit outage, so increasing $\psi_k[n]$ can only help by moving the user out of the sure-outage region.

The running-average goodput is updated as

$$\bar{q}_k[n+1] = (1-\beta_q)\bar{q}_k[n] + \beta_q r_k^{\mathrm{gp}}[n], \qquad 0 < \beta_q \le 1, \tag{23}$$

where the goodput of the scheduled user is its target rate scaled by the success probability and the fraction of the frame left after pilot overhead,

$$r_{k_n}^{\mathrm{gp}}[n] = R_{k_n}\big(1 - P_{\mathrm{out},k_n}[n]\big)\Big(1 - \tfrac{\tau_p\, t_{\mathrm{sym}}}{\Delta T_p}\Big), \tag{24}$$

with t_{sym} the pilot symbol duration, and $r_k^{\mathrm{gp}}[n] = 0$ for unscheduled users. The scheduled user is

$$k_n = \arg\max_{k\in\{1,\dots,K\}} \mathrm{score}_k[n]. \tag{25}$$

After selecting k_n, the radiator is updated by

$$y_r[n+1] = \Pi_{[0,D]}\Big(y_r[n] + \Pi_{[-v_r^{\max}\Delta t,\, v_r^{\max}\Delta t]}\big(y_{k_n}[n] - y_r[n]\big)\Big). \tag{26}$$

Let $\mathcal{Y}_n = [0, D] \cap \big[y_r[n] - v_r^{\max}\Delta t,\ y_r[n] + v_r^{\max}\Delta t\big]$.

Then (26) is equivalently $y_r[n+1] = \Pi_{\mathcal{Y}_n}(y_{k_n}[n])$.

Proposition 4 (One-step optimality of the motion update)**.** *For the scheduled user k_n, the update in* (26) *solves $y_r[n+1] = \arg\min_{y\in\mathcal{Y}_n} |y - y_{k_n}[n]|^2$.*

Hence, among all feasible next radiator positions satisfying the box and speed constraints, (26) *chooses the one closest to the scheduled user in the longitudinal direction.*

Proof. The set $\mathcal{Y}_n$ is a nonempty closed interval, and $y_r[n+1]$ in (26) is the Euclidean projection of $y_{k_n}[n]$ onto it.

The fast-timescale rule in (22)–(26) requires $O(K)$ operations per slot, while the slow-timescale pilot search evaluates $O(|\mathcal{T}|)$ candidates per adaptation epoch. This heuristic policy is an approximation resulting from (13)–(15), where the scheduler uses a monotone reliability proxy constrained by proportionally fair regularization, and the move in question is the nearest move possible for the scheduled user in one time step. Our scheme differs from previous approaches trying to address the problem using average or total rates under quasi-static channels. We make no claims about our approach being optimal or near-optimal for (20). The scoring criterion in (22) is merely a monotone approximation of the outage probability over one time step (see Proposition 3) but not of the horizon quantile J_α, so there is a gap here, which should be studied in the future.

VI. Numerical Results

We assume that $D = 120$ m, $K = 8$, $f_c = 28$ GHz, $x_r = 8$ m, $h_r = 6$ m, $\nu = 2.2$, $\alpha_{\mathrm{wg}} = 0.03$ dB/m, $\eta_c = 0.8$, $\Delta t = 0.5$ ms, mean speed $\bar{v} = 20$ m/s with standard deviation 2 m/s, $v_r^{\max} = 25$ m/s, $\rho_p = 15$, $\tau_p = 8$, pilot symbol duration $= 15\,\mu$s, and $R = 0.7$ b/s/Hz. All baselines apply the same system model in order to ensure fair comparisons. *Tracking-only* [12] utilizes the mobility capabilities of the PASS scheme without incorporating the CSI reliability metric in the scheduler function, *Fixed-PA PASS* [8] implements a fixed transmitter location which is optimal for reducing the level of attenuation, and the *Fixed RSU* [13] baseline employs the classical static roadside unit (RSU). Figs. 2 and 3 each employ 5000 time slots (of which the first 800 are used for warming up), computed with 32 seeds.

Fig. 2 shows the average outage probability versus nominal SNR for $\Delta T_p = 1$ ms. Note that the lines are based on the slot-wise closed-form outage expression in (13), whereas the markers use Monte Carlo (MC) simulation of scheduled-user states with explicit Rayleigh fading. This confirms the accuracy of (13). For an SNR of 20 dB, our scheme reduces

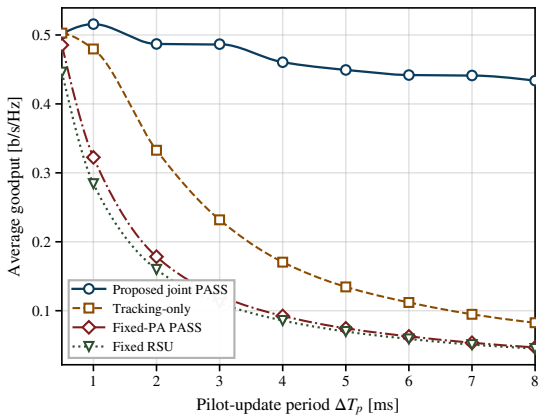

Fig. 3. Average goodput versus pilot-update period ΔT_p at SNR $= 20$ dB.

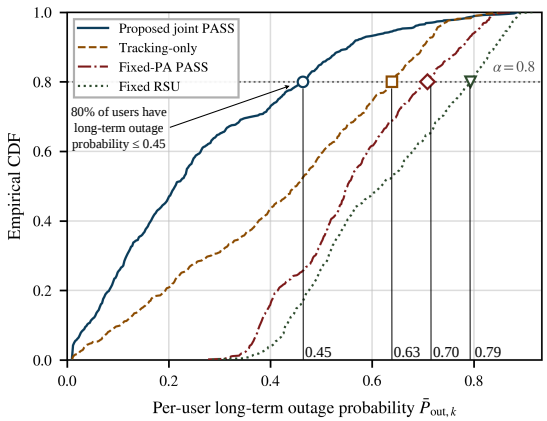

Fig. 4. Empirical CDF of the finite-horizon per-user outage metric $\hat{P}^{(N)}_{\text{out},k}$ at SNR $= 20$ dB and $\Delta T_p = 1$ ms.

outage from 0.232 (*Tracking-only*) to 0.160, i.e., a reduction of 31.0%. The improvement comes from using radiator motion to raise the CSI reliability ψ_k together with reliability-aware scheduling, not from mobility alone.

Fig. 3 shows average goodput versus pilot update period ΔT_p for SNR $= 20$ dB. Goodput is obtained from (24) by multiplying target rate, probability of success, and payload fraction after pilot overhead, then averaging over time and seeds. The line uses $\Delta T_p \in [0.5, 8]$ ms and the markers correspond to the candidate set $\mathcal{T}$, capturing the pilot-overhead/CSI-freshness trade-off in (21). At $\Delta T_p = 1$ ms, our scheme attains 0.516 b/s/Hz, outperforming *Tracking-only*'s 0.480 b/s/Hz by 7.5%.

Fig. 4 shows the user-level reliability via the empirical cumulative distribution function (CDF) of $\hat{P}^{(N)}_{\text{out},k}$, whose 0.8-quantile is the value below which 80% of user-level outages fall. The proposed scheme shifts the CDF left and reduces this quantile from 0.588 to 0.413, i.e., by 29.9%.

VII. Conclusion

We studied reliability-oriented mobility control for a PASS-assisted highway V2I system, where radiator motion shapes the propagation geometry and residual Doppler spread while the residual fast fading is Rayleigh-equivalent. The equivalent-SNR CSI reliability metric provides a conditional outage probability formula, a high-SNR outage floor, and a condition for an actuator limitation on the floor. Additionally, a quantile-based reliability measure was introduced, as well as a low-complexity policy for pilot update, scheduling, and mobility. Simulations have demonstrated significant improvements compared to the baselines. Next steps include LoS and NLoS blocking considerations and Rician fading.

Acknowledgment

This work was supported by the Department of Telecommunications (DoT), Government of India, and the Telecom Centres of Excellence (TCoE) India under the grant TCOE/TTDF/2025/140 through the Telecom Technology Development Fund (TTDF) Scheme on "Accelerated Research on 6G Ecosystem." The authors also acknowledge the support of the Machine Intelligence, Computing, and xG Networks (MICxN) Lab and the Stepwell High Performance Computing Facility at Ahmedabad University.

References

[1] Z. Wang, V. W. S. Wong, and R. Schober, "Integrated sensing and communications for end-to-end predictive beamforming design in vehicle-to-infrastructure networks," *IEEE J. Sel. Topics Signal Process.*, vol. 18, no. 5, pp. 933–949, 2024.

[2] Y. Han, W. Tang, X. Li, M. Matthaiou, and S. Jin, "CSI acquisition in RIS-assisted mobile communication systems," *Natl. Sci. Rev.*, vol. 10, no. 8, Art. no. nwad127, 2023.

[3] A. K. Papazafeiropoulos, I. Krikidis, and P. Kourtessis, "Impact of channel aging on reconfigurable intelligent surface aided massive MIMO systems with statistical CSI," *IEEE Trans. Veh. Technol.*, vol. 72, no. 1, pp. 689–703, Jan. 2023.

[4] A. Fukuda, H. Yamamoto, H. Okazaki, and Y. Suzuki, "Pinching antenna—using a dielectric waveguide as an antenna," *NTT DOCOMO Tech. J.*, vol. 23, no. 3, pp. 5–12, Jan. 2022.

[5] Z. Ding, R. Schober, and H. V. Poor, "Flexible-antenna systems: A pinching-antenna perspective," *IEEE Trans. Commun.*, vol. 73, no. 10, pp. 9236–9253, 2025.

[6] Y. Liu, Z. Wang, X. Mu, C. Ouyang, X. Xu, and Z. Ding, "Pinching-Antenna Systems (PASS): Architecture Designs, Opportunities, and Outlook," *arXiv preprint arXiv:2501.18409*, Jan. 2025.

[7] D. Tyrovolas, S. A. Tegos, P. D. Diamantoulakis, S. Ioannidis, C. K. Liaskos, and G. K. Karagiannidis, "Performance analysis of pinching-antenna systems," *arXiv preprint arXiv:2502.06701*, Feb. 2025.

[8] Y. Xu, Z. Ding, R. Schober, and T.-H. Chang, "Pinching-antenna systems with in-waveguide attenuation: Performance analysis and algorithm design," *arXiv preprint arXiv:2506.23966*, Jun. 2025.

[9] G. Zhou, V. Papanikolaou, Z. Ding, and R. Schober, "Channel estimation for mmWave pinching-antenna systems," in *Proc. IEEE 26th Int. Workshop Signal Process. Adv. Wireless Commun. (SPAWC)*, 2025, pp. 1–5.

[10] Y. Xu, Y. Lu, Z. Ding, and T.-H. Chang, "Pinching-Antenna System Design under Random LoS and NLoS Channels," *arXiv preprint arXiv:2512.04719*, Dec. 2025.

[11] R. H. Clarke, "A statistical theory of mobile-radio reception," *Bell Syst. Tech. J.*, vol. 47, no. 6, pp. 957–1000, Jul./Aug. 1968.

[12] V. P. Harigovindan, A. V. Babu, and L. Jacob, "Proportional fair resource allocation in vehicle-to-infrastructure networks for drive-thru Internet applications," *Comput. Commun.*, vol. 40, pp. 33–50, 2014.

[13] A. Guerna, S. Bitam, and C. T. Calafate, "Roadside Unit Deployment in Internet of Vehicles Systems: A Survey," *Sensors*, vol. 22, no. 9, Art. no. 3190, 2022.